Available online at www.sciencedirect.com
SCIENCE DIRECT®
Nitric Oxide 11 (2004) 263–272
NITRIC OXIDE Biology and Chemistry
www.elsevier.com/locate/yniox

S-Nitrosoglutathione incorporated in poly(ethylene glycol) matrix: potential use for topical nitric oxide delivery

Amedea Barozzi Seabra[a], Gabriela Freitas Pereira de Souza[a], Lilian Lúcia da Rocha[b], Marcos Nogueira Eberlin[b], Marcelo Ganzarolli de Oliveira[a,*]

[a] *Departamento de Físico-Química, Instituto de Química, Universidade Estadual de Campinas, UNICAMP, Campinas, SP, Brazil*
[b] *Laboratório Thomson de Espectrometria de Massas, Instituto de Química, Universidade Estadual de Campinas, UNICAMP, Campinas, SP, Brazil*

Received 24 June 2004; revised 22 September 2004

Abstract

Incorporation of nitric oxide (NO) donors in non-toxic polymeric matrices can be a useful strategy for allowing topical NO delivery. We have incorporated the NO-donor *S*-nitrosoglutathione (GSNO) into a liquid poly(ethylene glycol) (PEG)/H_2O matrix through the S-nitrosation of GSH by a NO/O_2 gas mixture. Kinetic measurements of GSNO decomposition associated with NO release were performed at 25, 35, and 45 °C in the dark and under irradiation with UV/Vis light, $\lambda > 480$ nm and $\lambda = 333$ nm. NO release from the liquid matrix to the gas phase was confirmed by mass spectrometry. The PEG/H_2O matrix stabilizes GSNO leading to expressive reductions in the initial rates of thermal and photochemical NO release, compared to aqueous GSNO solution. This matrix effect is assigned to diffusional constrains imposed on the escape of the NO and GS radicals formed in the solvent cage. This effect allows the storage of PEG-GSNO formulations for extended periods (more than 65 days at freezer) with negligible decomposition. PEG-GSNO formulation seems therefore to be applicable in topical NO delivery and GSNO displays potential as a percutaneous absorption enhancer. Moreover, the rate of NO release can be locally increased by irradiation with visible light.

Keywords: Nitric oxide; *S*-Nitrosothiols; *S*-Nitrosoglutathione; Poly(ethylene glycol); Photolysis; Radical recombination

Nitric oxide (NO) is an endogenous mediator of numerous physiological processes [1] such as the regulation of vascular tone [2], macrophage mediated neurotoxicity [3], platelet aggregation, [4], and neuronal transmission [5]. At low concentrations (nmol range), NO mediates several physiological functions, and larger amounts of NO (μmol range) are produced in some pathological states [6] such as in sepsis [7], diabetes [8], arthritis [9], and cancer [10]. Owing to several biological functions of NO, a great effort has been devoted to the development of NO delivering systems for pharmacological purposes such as those that provide local vasodilator or cytotoxic effects [11,12]. Compounds that act as NO carriers and can release NO in a controlled manner are thus of great relevance for such applications [13]. Endogenously found thiol-containing peptides, such as glutathione (GSH), are considered to be NO carriers and donors in mammals. In fact, GSH can undergo S-nitrosation reaction yielding *S*-nitroglutathione (GSNO), which belongs to a class of compounds named *S*-nitrosothiols (RSNOs) [14]. One of the main advantages of having NO carried as an RSNO is its preservation from inactivation caused by reaction with oxygen, leading to nitrite (NO_2^-) and nitrate (NO_3^-) [15]. The biological actions of RSNOs as vasodilators and as cytotoxic agents in killing malaria and leishmania parasites have already been demonstrated [16–18] and highlight their pharmacological potential.

In biological media, GSNO is able to deliver NO directly through transnitrosation reactions. However, the

* Corresponding author. Fax: +55 19 3788 3023.
E-mail address: mgo@iqm.unicamp.br (M.G. de Oliveira).

1089-8603/$ - see front matter © 2004 Elsevier Inc. All rights reserved.
doi:10.1016/j.niox.2004.09.005

previous release of free NO through the homolytic cleavage of the S–N bond, Eq. (1), can allow high concentrations of NO, locally, in levels that would be impossible to achieve by using NO gas or by promoting an increase in the endogenous synthesis of NO from L-arginine. The only byproduct in this thermal decomposition pathway is oxidized glutathione (GSSG).

$$2GSNO = 2NO + GSSG \quad (1)$$

The homolytic cleavage of the S–N bond of RSNOs, according to Eq. (1), can be accelerated through the irradiation of the molecules by UV/Vis light. This photochemical effect was already demonstrated in other works [19,20] and can be a useful strategy to increase the rate of NO release in local applications.

The potential pharmacological applications of RSNOs require, however, a vehicle since in aqueous solutions they decompose too fast to allow storage and handling, and solid pure RSNOs would find few, if none, applications. Non-toxic polymers already used as vehicles in pharmacological applications are the main candidates for carrying RSNOs [21]. The basic requirement is this strategy is that the matrix has to be a good solvent for RSNOs. Poly(ethylene glycol) (PEG), which has the general structural formula: $HO–(CH_2CH_2O)_n–CH_2CH_2OH$ (where n can range from 2 to ca. 180,000), dissolves polar molecules owing to polar and hydrogen bonding interactions with their ether oxygens and terminal hydroxyl groups. Despite its apparent simplicity, PEG has been the focus of much interest in biomedical and biotechnical communities [22]. In fact, many proteins, endogenous molecules, and drugs have been modified by covalent attachment to the PEG chain (Pegylation), such as superoxide dismutase [23], hemoglobin [24], endopeptidase [25], and catalase [26]. The pegylation can be extended to many other classes of compounds such as cytokines, blood factors, peptides, antifungal, antibiotics, anticancer, and immunosuppressive agents [27,28]. PEG has also been successfully used as a hydrogel matrix to provide localized and sustained NO release [29,30], as a medium for encapsulation of nanoparticles for pharmaceutical purposes [31], as a constitutive matrix for nanoparticles for mucosal delivery of proteins and plasmid DNA [32], as a component of micellar formulations for drug delivery [33,34], and as a film for microdevices [35]. PEG not only allows controlled release of several drugs, but it also widely used for biomedical applications for its biocompatibility and easy manipulation. PEG is transparent, so it is also possible to irradiate the incorporated drugs in PEG matrices for phototherapeutic applications.

In the present work, the NO-donor GSNO was incorporated in PEG 200 matrix. The kinetics of thermal and photochemical NO release from GSNO in this formulation was monitored and compared to the kinetics in aqueous solutions in three different temperatures. It was found that PEG matrix reduces the rates of both thermal and photochemical NO release from GSNO, in comparison with those found in aqueous solutions. This stabilization effect is discussed on the basis of a cage recombination mechanism. The potential of this formulation for the topical delivery of NO, and its storage properties are also discussed.

Experimental procedure

Materials

Poly(ethylene glycol) (PEG) (average M_n ca. 200) (Aldrich Chemical, USA), glutathione (γ-Glu-Cys-Glu, GSH) (Sigma, St. Louis, MO) were used as received. Gaseous NO was obtained from a gas cylinder (White Martins, Campinas, SP, Brazil). Synthetic air (N_2/O_2, 79/21 v/v, $H_2O < 2$ ppm, THC, $CO + CO_2 < 0{,}3$ ppm) was purchased from Air Liquide, Campinas, SP, Brazil. All the experiments were carried out using analytical grade water from a Millipore Milli-Q Gradient filtration system.

Preparation of PEG/H_2O-GSH solutions

Aqueous solutions of GSH (46.5 mmol L^{-1}) were prepared by direct dissolution of solid dry GSH in water. Due to the low solubility of GSH in pure PEG-200 matrix, GSH was previously dissolved in a small amount of distilled-deionized water, to yield a concentrate (0.527 mol L^{-1}) solution of GSH. This solution was then added to a pre-measured volume of PEG-200 and stirred at room temperature, until the achievement of a homogeneous translucent solution. The volume ratio PEG-200:H_2O in this solution was 9.6:1 v/v with a final concentration of GSH of 46.5 mmol L^{-1}.

Synthesis of GSNO in aqueous solution and in PEG matrix

The synthesis of GSNO either in aqueous solution or in PEG/H_2O matrix was achieved by bubbling a mixture of NO/synthetic air through GSH solutions in a quartz spectrophotometer cuvette. The gaseous mixture was prepared by mixing NO from a gas cylinder with O_2 from a cylinder of synthetic air. The gas flows were controlled by flowmeters (Aldrich) to give a mixture with a known NO/O_2 ratio. Pre-adjusted ratios of NO:O_2 1:1 v/v (5.6:5.6 mL min^{-1}) were used. Reactions were performed in a thermostatized quartz cuvette with a Teflon stopper crossed by four polypropylene tubes, which delivered the gas mixture to the bottom of the cuvette. A solenoid valve (Cole Palmer) controlled by an electronic circuit developed for this purpose was used to produce gas pulses with pre-adjusted frequency and

duration. Gas pulses were typically of 2.1 s for aqueous solutions and 3.0 s for PEG matrix, delivered at a frequency of 0.48 s^{-1} (aqueous solutions) and 0.33 s^{-1} (PEG matrix). The reaction was followed spectroscopically using an HP 8453 diode array Spectrophotometer (Hewlett–Packard, model 8453, Palo Alto, CA, USA). The syntheses of GSNO were monitored at $\lambda = 545$ nm, which corresponds to the maximum of its visible absorption band. This band was observed to increase continuously with the total time of bubbling until a maximum was reached. S-nitrosation was carried out until the achievement of this maximum to ensure a complete reaction and to avoid an excess of the nitrosating reactant.

Kinetic measurements of GSNO decomposition with NO release

Spectral changes of GSNO in aqueous solution and in PEG matrix in the range of 220–1100 nm were monitored in the dark and under irradiation conditions. All the spectra acquisitions were monitored using a temperature-controlled sample holder. Kinetic curves of thermal and photochemical decomposition of GSNO were obtained from the absorption changes at 545 nm. Kinetic data were taken at this wavelength in 10 min intervals at 25, 35, and 45 °C referenced against air.

The amount of NO released over time was calculated directly from the amount of GSNO decomposed. This calculation was based on the fact that the decay of the absorption bands of GSNO at 545 nm can be associated solely to the homolytic cleavage of the S–N bond with NO release, according to Eq. (1) [20]. Thus, the increase in the concentration of NO released over time ($[NO]_t$) was calculated from the changes in GSNO concentration ($[GSNO]_0 - [GSNO]_t$), according to Beer's law:

$$[NO]_t = [GSNO]_0 - [GSNO]_t = (A_0 b/\varepsilon_{GSNO}) - (A_t b/\varepsilon_{GSNO}), \quad (2)$$

where A_0 and A_t are the GSNO absorbances at 545 nm at the beginning of the monitoring and at time t, respectively, $[GSNO]_0$ and $[GSNO]_t$ are the concentrations of GSNO at the beginning of the reaction and at time t, respectively, ε_{GSNO} is the molar absorption coefficient of GSNO at 545 nm, which was calculated as $\varepsilon_{GSNO} = 16.1\ mol^{-1}\ L^{-1}\ cm^{-1}$ [36,37], and b is the optical path (1 cm). Therefore, by measuring the kinetics of absorbance of GSNO in aqueous solution and in PEG matrix it was possible to obtain the kinetics of NO release from GSNO.

Initial rates (I_R) of thermal and photochemical NO release from GSNO were obtained by linear regression of the slopes of the initial sections (less than 10% of the reaction) of the NO concentration versus time plots according to

$$I_R = \Delta[NO]/\Delta t, \quad (3)$$

where $\Delta[NO]$ and Δt are the changes in NO concentration and the corresponding time intervals, respectively. Whenever possible, the kinetic curves of NO released versus time were fit to a first order exponential growth, according to

$$[NO]_t = [NO]_f - [NO]_f e^{-kt}, \quad (4)$$

where $[NO]_t$ is the NO concentration at each time t, $[NO]_f$ is the final NO concentration, and k is the first order rate constant. Each point in the kinetic curves represents the average of two experiments, with the error bars expressed by their standard error of the mean (SEM).

Irradiation of GSNO in aqueous solution and in PEG matrix

GSNO in aqueous solution and in PEG matrix were irradiated in quartz cuvettes from the top directly inside the sampling compartment of the spectrophotometer. A 125 W mercury-arc lamp (Philips, São Paulo, Brazil) (Fig. 1E-1) equipped with a 10 cm circulating-water filter (Oriel Instruments, Stratford, CT) (Fig. 1E-2) was used. A narrow irradiation band centered at 333 nm was selected using a prism monochromator (Carl Zeiss M4-QIII, Oberkochen, Germany M4-QIII) with exit slit width of 2 mm. Irradiation with $\lambda > 480$ nm was achieved by using a glass filter (GG-475—Schott Optical Glass—Duryea, PA) (Fig. 1E-3) and was performed in two different conditions: non-attenuated and attenuated with an iris diaphragm to achieve the same light intensity obtained with the prism monochromator. Irradiation with unfiltered light was carried out using the same assembly without filter. The light illumination periods were controlled with an electromechanical shutter (Oriel). A liquid light guide (Oriel) (Fig. 1E-4) was used for conducting light to the top of the cuvette. The same irradiation assembly was used for irradiating PEG-GSNO for mass spectrometry measurements. The intensities of light in all irradiation conditions were measured with a radiometer (Newport 1830-C Optical Power Meter, Irvine, CA, USA). Readings at the four irradiation conditions used were: (a) monochromator (at $\lambda = 333$ nm) = 33 nW cm^{-2}, (b) filter ($\lambda > 480$ nm) = 0.37 μW cm^{-2}, (c) filter ($\lambda > 480$ nm) with light intensity attenuated to 33 nW cm^{-2}, and (d) unfiltered light $\lambda = 6.5$ μW cm^{-2}. In each specific condition, the same light intensities were used in irradiations in PEG and aqueous solution.

The quantum yield for the photodecomposition of GSNO solutions (irradiated with 333 nm, selected by the monochromator) was determined by comparative actinometry using (*E*)-α-(2,5-dimethyl-3-furylethylidene)(isopropylidene) succic anhydride (AB) (Aberchromics, Cardiff, UK) as a reference [38]. AB undergoes

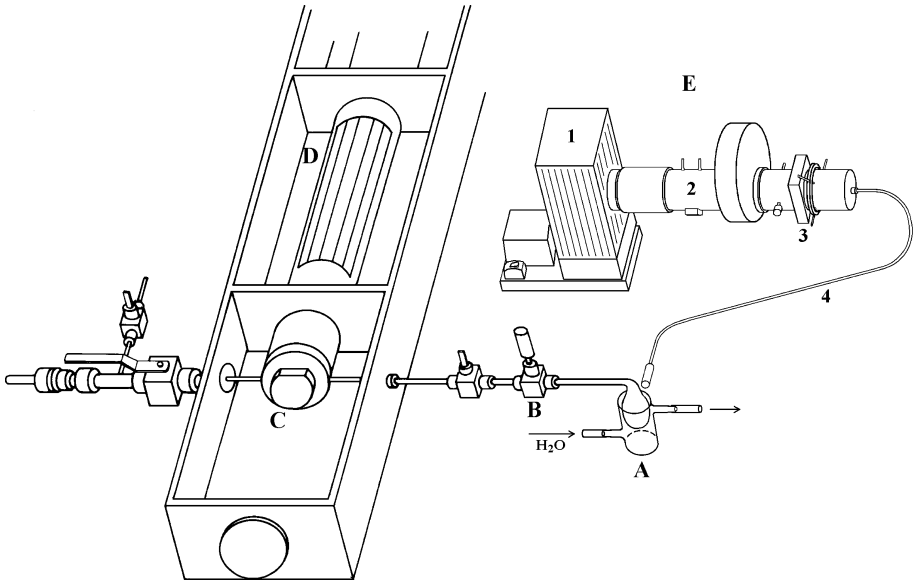

Fig. 1. System used for MS detection of free NO in the nearly air-free headspace of liquid PEG and PEG-GSNO solutions. (A) Thermostatized ampoule containing the samples; (B) needle valve; (C) EI ion source of the mass spectrometer; (D) high-transmission 3/4 in. mass analyzer quadrupole; and (E) Irradiation system: (1) mercury-arc lamp, (2) water filter, (3) holder for optical glass filter, and (4) liquid light guide.

conrotatory ring-closure to give deep red 7,7a-dihydro-2, 4,7,7,7a-pentamethylbenzo[*b*] furan-5,6-dicarboxylic anhydride (DHBF) under irradiation in toluene, in the range 313–366 nm. This photochromic molecule has a quantum yield for photocoloration, Φ_{AB}, of 0.20 over the range 313–336 nm and a molar adsorption coefficient, ε_{DHBF}, of 8200 $mol^{-1}\,L^{-1}\,cm^{-1}$ at 494 nm [38]. An accurately measured volume (V) of a solution of AB in toluene at a concentration of 4.80 mmol L^{-1} was exposed to irradiation with $\lambda = 333$ nm for a measured time (t) and the increase in absorbance (ΔA) at 494 nm was determined. The radiant flux of the lamp (I) was calculated to be 3.30×10^{14} photons s^{-1} from Eq. (5), where N is the Avogadro number

$$I = \frac{\Delta A V N}{\Phi_{AB}\varepsilon_{DHBF} t}. \quad (5)$$

The quantum yields for the overall loss of GSNO, ϕ_{GSNO}, were determined according to Eq. (6)

$$\theta_{GSNO} = \theta_{AB}\left(\frac{\Delta A_{GSNO}\varepsilon_{AB} V_{GSNO} t_{AB}}{\Delta A_{AB}\varepsilon_{GSNO} V_{AB} t_{GSNO}}\right). \quad (6)$$

Mass spectrometry measurements

A diagram of the MS system used for NO monitoring is shown in Fig. 1. Volumes of 500 μL of liquid PEG-GSNO (46.5 mmol L^{-1}) or the control (pure PEG) were placed into a small ampoule (A), which was connected, via a needle valve and a 1/4 in. stainless-steel line (B), to the ion source of the mass spectrometer (C). The ampoule (A) was placed inside a double-walled water-circulating flask (protected against ambient light) connected to a thermostatic bath and measurements were performed at 25 °C. The samples were monitored in dark conditions and under irradiation with $\lambda > 480$ nm, with the needle valve opened (Fig. 1E). The distance between the end of the light guide and the top of the solution inside the ampoule was ca. 5 cm.

An AAB Extrel (Pittsburgh, PA) quadrupole mass spectrometer described in details elsewhere [39] fitted with a high-transmission 3/4 in. mass analyzer quadrupole (D) was used. MS detection was performed using 70 eV electron ionization (EI). Mass spectra were first acquired in the range of m/z 24 to m/z 200 to screen for any gaseous compound, and then from m/z 26 to m/z 34 to selectively monitor the continuous release of NO (detected in its ionized form NO^+ of m/z 30) from the PEG-GSNO solutions.

Real time MS monitoring of NO based on the absolute intensity of the ion of m/z 30 for a period of 1 h from 500 μL of PEG-GSNO (46.5 mmol L^{-1}) placed in the ampoule was performed under irradiation with $\lambda > 480$ nm at 25 °C, with the needle valve completely opened.

Results and discussion

Synthesis of GSNO in aqueous solution and in PEG matrix

The synthesis of GSNO through the S-nitrosation reaction of GSH in aqueous solution and in PEG matrix was characterized by following the two absorption bands of GSNO at 336 and 545 nm. Both bands are

associated with the S–NO bond and have already been assigned to $\pi \rightarrow \pi^*$ and $n_N \rightarrow \pi^*$ transitions, respectively [14]. The visible band at 545 nm was chosen to monitor the kinetics of formation and cleavage of the S–N bond of GSNO in all the experiments. Fig. 2 shows the kinetic curves corresponding to the increase of the band at 545 nm, owing to formation of the S–NO bond. Each absorption datum was obtained after bubbling GSH aqueous solutions with the nitrosating NO/synthetic air gaseous mixture, as described in the experimental section. For a constant bubbling condition, the rates of nitrosation are low in the initial sections of the curves (until ca. 20 s in water and 50 s in PEG/H_2O) and then increase steeply until the maximums are reached. The lower rates of nitrosation in the beginning of the bubbling can be assigned to the time necessary to attain an equilibrium concentration of the dissolved gases in the liquid matrices. This initial section is, as expected, longer in the PEG matrix than in aqueous solution, once the former media have a much higher viscosity, and therefore limit the diffusion of the gases and the attainment of an equilibrium concentration. The effect of the higher viscosity of PEG is also reflected in the greater error bars of the corresponding curve in Fig. 2, which are due to the light scattering caused by small bubbles rising slowly through the cuvette, during data acquisition.

The S-nitrosation reaction of GSH in aqueous solution and in PEG/H_2O by bubbling a gaseous mixture of NO/synthetic air is known to produce dinitrogen trioxide (N_2O_3), which is responsible for S-nitrosating GSH [20], according to the following reaction:

$$N_2O_3 + GSH = GSNO + NO_2^- + H^+ \quad (7)$$

Nitrite formed is expected to hydrolyze and to establish the following equilibrium:

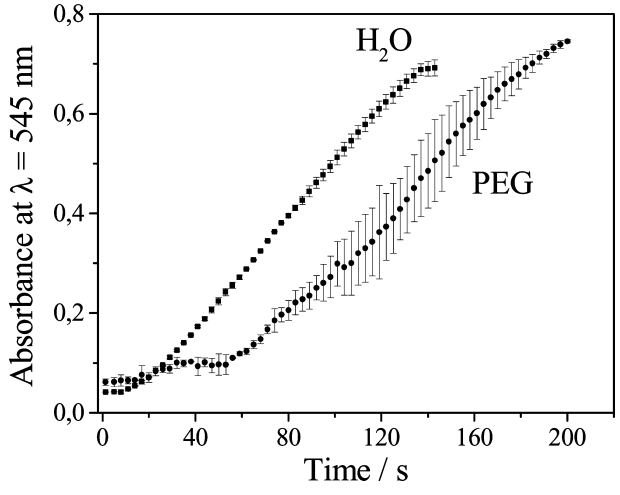

Fig. 2. Kinetic curves monitored at 545 nm corresponding to the synthesis of GSNO by bubbling a gaseous NO/synthetic air mixture through GSH (46.5 mmol L^{-1}) in aqueous solution and in PEG matrix, as indicated in the figure.

$$NO_2^- + H^+ = HO - NO = OH^- - NO^+ \quad (8)$$

S-nitrosation of GSH can also proceed through the nucleophilic attack of the nitrosonium cation (NO^+) to the sulfur atom of the thiol group, yielding a further GSNO molecule and water (Eq. (9))

$$OH^- - NO^+ + GSH = GSNO + H_2O \quad (9)$$

The overall reaction can thus be written as

$$N_2O_3 + 2GSH = 2GSNO + H_2O \quad (10)$$

This method allows the in situ nitrosation of GSH molecules previously dissolved in the PEG matrix and displays several advantages over the usual nitrosation methods, based on the use of sodium nitrite in acidic medium (hydrochloric acid). This in situ nitrosation method requires no water addition to the polymeric matrix other than the small amount of water used to the previous dissolution of GSH, as described above; hence, viscous PEG formulations often advantageous for pharmaceutical applications can be obtained. Avoiding the use of $NaNO_2$ and HCl implies also that possible impurities present in such reactants are eliminated. Impurities introduced into the matrix by using analytical grade NO and synthetic air are surely substantially reduced because only gaseous impurities can reach the matrix. In addition, the gases can be purified by simple bubbling procedures to remove gaseous impurities. The final solutions obtained are transparent, allowing the monitoring of GSNO concentration. GSNO monitoring is a further advantage of this method not only by allowing one to characterize formulation stability, but also to allow precise end point control of the reaction, hence the use of an excess of the nitrosating reactants is avoided.

Thermal NO release from GSNO in aqueous solution and in PEG matrix

GSNO incorporated in PEG matrix and in aqueous solution showed continuous decomposition with consequent NO release. GSNO decomposition was followed by the spectral changes associated with its absorption band at 545 nm. The band at 336 nm was not used because it was out of scale in the GSNO concentration used. The disappearance of each of these bands in the dark or under irradiation can be assigned to the homolytic cleavage of the S–N bond, giving rise to free NO and glutathione oxidized (GSSG) in a first order kinetics, according to the following equations [14,30]:

$$GSNO \rightarrow GS^{\bullet} + NO^{\bullet} \quad (11)$$

$$GS^{\bullet} + GSNO \rightarrow GSSG + NO^{\bullet} \quad (12)$$

The overall reaction is

$$2GSNO \rightarrow GSSG + 2NO^{\bullet} \quad (13)$$

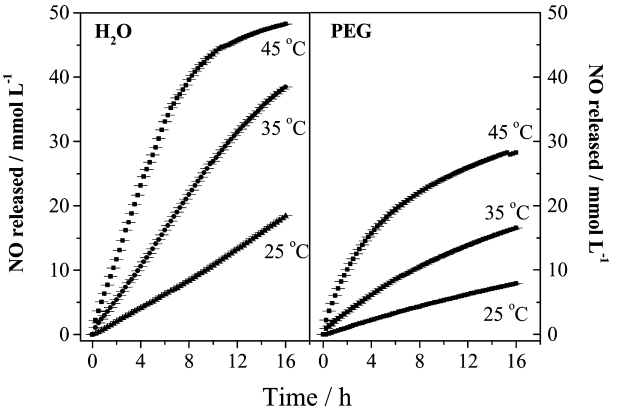

Fig. 3. Kinetic curves of NO release from GSNO (46.5 mmol L^{-1}) in aqueous solution and in PEG matrix in the dark at 25, 35, and 45 °C. The increases in the concentration of NO were calculated from the corresponding decomposition curves monitored at 545 nm (for details see Experimental procedure).

Fig. 3 shows the kinetic curves of thermal NO release from GSNO in aqueous solution and in PEG matrix at 25, 35, and 45 °C. It can be seen that the rates on NO release increase with temperature in both matrices, what is in accordance with a thermal decomposition process. A comparison among the magnitudes of the initial rates of NO release calculated from these curves is shown in the bar graphics of Fig. 4, making clear that a stabilization effect is achieved in PEG matrix in all temperatures relative to aqueous solutions. Table 1 shows the rate constants (k) of NO release in PEG matrix and the initial rates (I_R) of NO release in both PEG matrix and aqueous solution at 25, 35, and 45 °C. It can be seen that k values in PEG matrix increased 6.0 times with the increasing of temperature from 25 to 45 °C, with a corresponding increase of 7.7 times in the I_R values. The increase in I_R values in aqueous solutions is ca. five times in the same temperature range (k values could not be calculated for aqueous solutions). These figures indicate an important thermal responsivity of GSNO

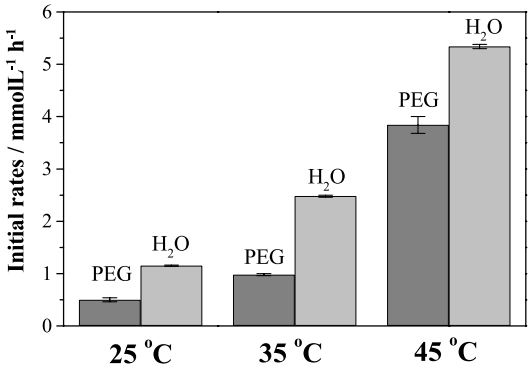

Fig. 4. Initial rates of NO release from GSNO (46.5 mmol L^{-1}) in aqueous solution and in PEG in the dark at 25, 35, and 45 °C. Rates were calculated from the kinetics curves of Fig. 3.

Table 1
First order rate constants (k) and initial rates (I_R) of NO release from GSNO (46.5 mmol L^{-1}) in PEG matrix and in aqueous solutions at 25, 35, and 45 °C[a]

Reaction conditions	$k \times 10^{-2}$ (h^{-1})	I_R (mmol L^{-1} h^{-1})
Aqueous solution		
25 °C	—	1.10 ± 0.01
35 °C	—	2.48 ± 0.02
45 °C	—	5.34 ± 0.04
PEG		
25 °C	2.8 ± 0.1	0.50 ± 0.04
35 °C	6.6 ± 0.1	0.98 ± 0.02
45 °C	16.8 ± 0.4	3.84 ± 0.16

[a] Activation energy of NO release from GSNO in PEG matrix = 68 ± 3 kJ mol^{-1}. Apparent activation energy of NO release from GSNO in aqueous solution = 60.5 ± 4 kJ mol^{-1}.

in both aqueous and PEG matrices. The activation energy for the thermal cleavage of the S–N bond of GSNO with NO release, was estimated from k values obtained in the PEG matrix as 68 ± 3 kJ mol^{-1}. An estimate of the apparent activation energy in aqueous solution in the same temperature range led to the value of 60.5 ± 4 kJ mol^{-1}. Although several approximations are implied in these calculations, they lead to values with the same order of magnitude in the cases and can be taken as a reference for further comparisons with other NO donors in these matrices. The small difference in the activation energy can be taken as an indication that the same decomposition mechanism is operative in both matrices.

Photochemical NO release from GSNO in aqueous solution and in PEG matrix

Fig. 5 shows the kinetic curves of NO release from GSNO in aqueous solution and in PEG matrix in the dark, under irradiation with $\lambda = 333$ nm, $\lambda > 480$ nm, and $\lambda > 480$ nm attenuated and UV/Vis light (200–900 nm) at 25 °C. A comparison among the magnitude of the initial rates of thermal and photochemical NO releases calculated from these curves is shown in the bar graphic of Fig. 6. The initial rates of NO release from GSNO were found to be 1.8, 2.6, 5.1, 1.4, and 3.9-fold decreased in PEG matrix compared to the rates obtained in aqueous solutions in the dark and under irradiation with $\lambda = 333$ nm, $\lambda > 480$ nm, and $\lambda > 480$ nm attenuated and UV/Vis, respectively. Clearly, different irradiation conditions lead to different rates of NO release from GSNO in aqueous solution in both matrices. Despite the higher molar absorption coefficient of GSNO at 336 nm compared to the molar absorption coefficient at 545 nm, irradiation with $\lambda > 480$ nm is much more efficient for increasing the rate of NO release from GSNO, in comparison with irradiation with $\lambda = 333$ nm. This apparently conflicting result can be ex-

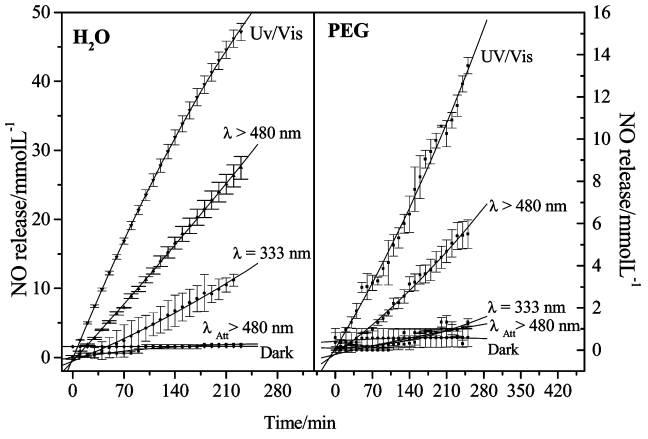

Fig. 5. Kinetic curves of NO release from GSNO (46.5 mmol L^{-1}) in aqueous solution and in PEG matrix at 25 °C in the dark, under irradiation with: $\lambda = 333$ nm (light intensity = 33 nW cm^{-2}), $\lambda > 480$ nm (light intensity = 0.37 μW cm^{-2}), $\lambda_{Att} > 480$ nm (light intensity attenuated to 33 nW cm^{-2}), and in the UV/Vis region (UV/Vis, light intensity = 6.5 μW cm^{-2}). The increases in the concentration of NO were calculated from the corresponding decomposition curves monitored at 545 nm (for details see Experimental procedure).

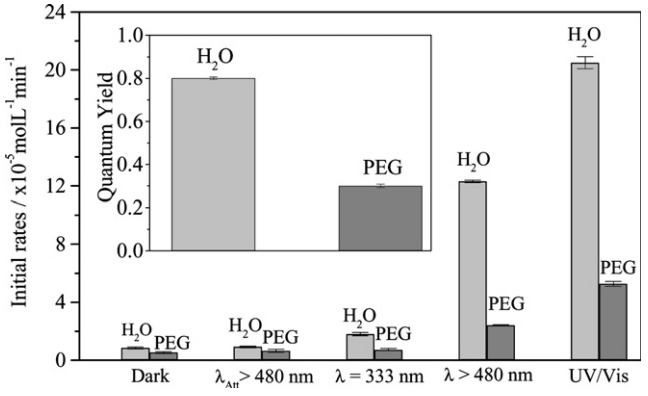

Fig. 6. Initial rates of NO release from GSNO (46.5 mmol L^{-1}) in aqueous solution and in PEG matrix at 25 °C in the dark, under irradiation with $\lambda_{Att} > 480$ nm (light intensity attenuated to 33 nW cm^{-2}), $\lambda = 333$ nm (light intensity = 33 nW cm^{-2}), $\lambda > 480$ nm (light intensity = 0.37 μW cm^{-2}), and in the UV/Vis region (light intensity = 6.5 μW cm^{-2}). Rates were calculated from the kinetic curves of Fig. 5. Inset: Quantum yield of NO release due to the photolysis of GSNO (46.5 mmol L^{-1}) with $I_R = 333$ nm in PEG matrix and in aqueous solution, at 25 °C.

plained by remembering that the prism monochromator used in the irradiation with $\lambda = 333$ nm greatly reduces the intensity of the light source compared to the intensity obtained with the filter ($\lambda > 480$ nm). The rate of NO release from GSNO under irradiation with $\lambda > 480$ nm with attenuated light intensity is very close to the rate found in dark condition, once the light intensity at this irradiation condition is very low and the molar absorption coefficient of GSNO is also low at the 545 nm band. Comparing the rates of NO release obtained at $\lambda > 480$ nm with those obtained at $\lambda = 333$ nm (at the same light intensity), one can see that the UV band is more photoactive than the visible band, due to its higher molar absorption coefficient. In addition, the difference between the rates of NO release at these two irradiation wavelengths is more prominent in aqueous solution than in PEG, due to the stabilizing effect of PEG.

The acceleration of the NO release reaction observed in aqueous solution and in PEG matrix through the irradiation with $\lambda = 333$ nm and with $\lambda > 480$ nm can be assigned to the promotion of the electronic transitions $\pi \rightarrow \pi^*$ and $n_N \rightarrow \pi^*$, respectively. These transitions weaken the S–N bond by populating the anti-bonding π^* orbital, leading to the bond cleavage with NO ejection. Evidently, irradiation of GSNO in the UV/Vis region is responsible for the promotion of both $\pi \rightarrow \pi^*$ and $n_N \rightarrow \pi^*$ electronic transitions, leading to an extra-increase in the rate of NO release. These different rates of NO from GSNO under these irradiations conditions indicate that the quality and the intensity of the light source be can be used as a tool to modulate the rate of NO release from the GSNO solutions.

The photochemical stabilization effect obtained in the PEG matrix was confirmed by obtaining the quantum yields (Φ) of photodecomposition under irradiation with $\lambda = 333$ nm, as shown as shown in the inset of Fig. 6. The Φ value for NO release from GSNO was found to be 2.7-fold higher in aqueous solution compared to the value found in the PEG matrix. The magnitude of Φ value obtained for the photodecomposition of GSNO in aqueous solution is in accordance with the value reported by Wood et al. [19], calculated by comparative actinometry.

Stabilization effect promoted by the PEG matrix on the rate of thermal and photochemical NO release from GSNO

The results showed that PEG matrix stabilizes the rate of NO release from GSNO in comparison with that observed in aqueous solution The stabilization effect promoted by the PEG microenvironment on the kinetics of NO release is also evident in the calculated extent of GSNO decomposition in PEG matrix in comparison with the values obtained in aqueous solutions (5 and 10% in the dark, respectively). This extent was calculated based on the extent of disappearance of the band at 545 nm for a total time period of 4 h. A similar difference in the extent of GSNO decomposition between the matrices was observed under irradiation with $\lambda > 480$ nm (18 and 55% for water and PEG, respectively) in the same time period.

We have already reported a reduction in the rates of thermal and photochemical NO release from the *S*-nitrosothiol *S*-nitroso-*N*-acetylcysteine (SNAC) in PEG matrix [20]. The effect, which can be assigned to the

geminate radical pair recombination after the primary homolytic (thermal or photochemical) cleavage of the S–N bond, also applies in the case of GSNO. The geminate recombination reaction between the two radicals formed (NO$^{\bullet}$ and GS$^{\bullet}$) is expected to be favored by the increase in the microviscosity of the solvent, while the fragments are still inside the solvent cage. The increased viscosity of the matrix also favors the non-geminate recombination of the fragments that escape solvent cage. Such effect is also important once the small NO molecules are expected to diffuse rapidly to the gas phase. By providing a less polar environment and a higher viscosity, PEG favors an increased residence time of free NO in the liquid phase, increasing the probability of random recombination with GS radicals that still did not react to form dimmers. The temperature effect on the reaction can also be interpreted through this mechanism. Thus, the reduction in the rates of GSNO decomposition with the lowering of temperature is not only a consequence of the reduction in the thermal energy available for the cleavage of the S–N bond, but also a reflex of the increase in the viscosity of the matrix. As a general consequence, PEG matrices have a great potential to store RSNOs at low temperatures, in the dark, for biomedical purposes. In fact, PEG-GSNO formulations can be storage for more than 65 days at freezer without GSNO decomposition with consequent NO release, while 87% of GSNO decomposes releasing NO at 8 °C. Thus, the control of temperature is important to storage PEG-GSNO formulations. In addition, as PEG matrices are water soluble, dilute aqueous solutions could be prepared from concentrate PEG-GSNO stock solutions.

Detection of free NO released from PEG-GSNO by mass spectrometry

Mass spectrometry (MS) is particularly suitable for direct detection and characterization of gases and gas mixtures with high sensitivity and selectivity [40–42], and MS has also been employed to detect trace amounts of NO released directly from solid materials to the gas phase. For instance, MS with a modified dynamic fast atom bombardment (FAB) probe technique has been used to detect NO and other gaseous products released in the photochemical decomposition of sodium nitroprusside (SNP) in aqueous solution [43]. Although other techniques identify and quantify NO [44–47], MS represents one the most sensitive and selective techniques to confirm free NO release from solid or liquid biomaterials to the gas phase. Fig. 7 shows the evolution of the 70 eV EI mass spectra in the m/z 26–34 range used to monitor continuously the headspace composition above the liquid PEG-GSNO solutions at 25 °C in the dark and under irradiation with $I_R > 480$ nm. The "blank mass spectra" of the headspace gas obtained with pure

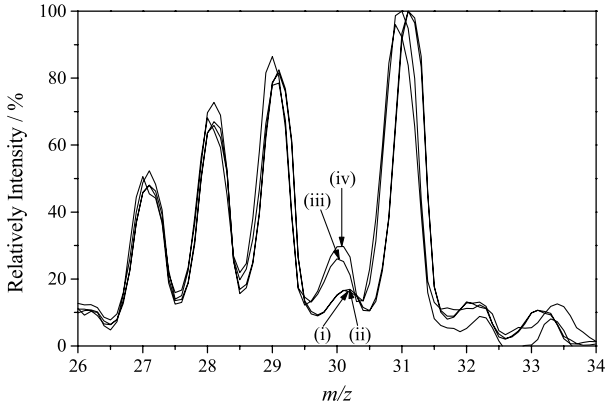

Fig. 7. EI mass spectra (70 eV) in the m/z 26–34 range. (i) Blank mass spectrum of the headspace gas obtained with 500 μL of pure PEG 200 in the dark and (ii) after 20 min of irradiation with $\lambda > 480$ nm. (iii) Mass spectra for PEG-GSNO solutions (46.5 mmol L^{-1} of GSNO) in the dark and (iv) after 20 min of irradiation with $\lambda > 480$ nm. Temperature was kept in 25 °C. Note for the PEG-GNSO solutions the raising upon irradiation of the m/z 30 ion peak ($^{14}N^{16}O^{+}$) assigned to the detection of free NO.

PEG in the dark (i) and under irradiation with $\lambda > 480$ nm (ii) display mainly ions of m/z 27, 28, 29, 30.3, 31, 32, and 33. The ions of m/z 28 and 32 are present in an abundance ratio of near 4:1, owing therefore to residual air, that is, $^{14}N_2^{+\bullet}$ of m/z 28 and $^{16}O_2^{+\bullet}$ of m/z 32. Despite high vacuum (10^{-7} Torr) cleanup of the headspace region, air is still present, although in very low concentrations, therefore, its main components are still clearly detected by MS. The other ions of m/z 27, 29, 30.3, 31, and 33 are likely arising from fragments of ionized PEG fragments. As curves (i) and (ii) in Fig. 7 are nearly identical, there is no chemical effect of irradiation with $\lambda > 480$ nm on pure PEG, as expected.

PEG-GSNO mass spectrum clearly displays, however, an additional and relatively abundant ion of m/z 30, $^{14}N^{16}O^{+}$, which can be assigned to the detection of free NO. The intensity of the m/z 30 ion peak increases under irradiation with visible light (iv) in comparison with the dark condition (iii). This result shows that free NO is spontaneously released from the PEG-GSNO solutions in the dark, and that the rate of NO release increases with irradiation with $\lambda > 480$ nm, in accordance with the kinetic measurements herein reported. MS monitoring confirms therefore that NO is released through the homolytic bong cleavage of the S–N bond of GSNO incorporated in PEG matrix according to Eq. (1).

Fig. 8 shows the real time MS monitoring of NO as detected by its ionized form NO^{+} of m/z 30 from PEG-GSNO, at 25 °C under irradiation with $\lambda > 480$ nm. The m/z 30 ion current increases continually during the 40 min of irradiation. As the lamp is turned off, the NO^{+} current decreases immediately in a continuous pattern. This result provides additional evi-

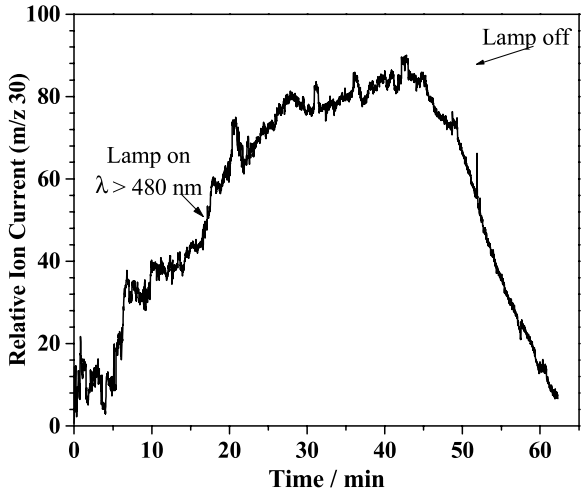

Fig. 8. Real time monitoring of the m/z 30 ($^{14}N^{16}O^{+}$) ion current from the headspace of 500 μL PEG/H_2O-GSNO solution containing 46.5 mmol L^{-1} of GSNO at 25 °C under irradiation with $\lambda > 480$ nm.

dence that irradiation of PEG-GSNO with visible light increases the rate of NO release and is in accordance with the increased NO release measured on the bases of GSNO decay, also discussed previously.

Potential uses for topical applications and for percutaneous absorption enhancement

The incorporation of the NO donor GSNO in PEG matrix may represent a new strategy for topical application and local vasodilatation. We have recently reported the local increase of blood flow with the topical application of GSNO-containing hydrogels of poly(ethylene glycol)–poly(propylene glycol)–poly(ethylene glycol) (PEO–PPO–PEO) in the forearm of human subjects [12]. The chemical similarity between this formulation and the PEG-GSNO formulation herein reported includes not only the NO donor (which is the same) but also the polymeric matrix. In addition to the above-mentioned advantages of using PEG in pharmaceutical formulations, PEG itself is considered to be a skin penetration enhancer [48]. Therefore, its association with GSNO, which acts by increasing the local blood flow, may provide an efficient strategy to enhance the skin penetration and the percutaneous absorption of other therapeutic agents, in a combined administration.

Conclusion

GSNO can be synthesized directly in PEG matrix via S-nitrosation of incorporated GSH. GSNO is found to be a spontaneous NO-donor, in both aqueous solution and PEG matrix. The thermal NO release reaction of GSNO has been confirmed by increase in the initial reaction rate with temperature increase in both mediums and by MS and spectroscopic analysis. Homolytic cleavage of the S–N bond has been determined as the pathway of NO release from GSNO incorporated in PEG. The rate of photochemical NO release from GSNO is increased by irradiation in the UV or visible absorption bands of GSNO, or both, with sources of different wavelength ranges and may increase rates of topical NO release. The stabilization effect obtained in PEG matrix relative to aqueous solution in the dark and under irradiation was assigned to the cage effect imposed by the viscous matrix and may allow both the modulation of the rate of NO release and the storage of GSNO solutions in a non-toxic matrix.

Acknowledgments

We thank the São Paulo State Research Foundation (FAPESP) and the Brazilian National Research Council (CNPq) for financial support. ABS, GFPS, and LLR thank FAPESP for graduate fellowships (01/7869-9; 04/00819-0; and 99/08006-9). We thank Mr. Iveraldo Rodrigues for drawing Fig. 1.

References

[1] E. Nisoli, E. Clementi, C. Paolucci, V. Cozzi, C. Tonello, C. Sciorati, R. Bracale, A. Valerio, M. Francolini, S. Moncada, M.O. Carruba, Mitochondrial biogenesis in mammals: the role of endogenous nitric oxide, Science 299 (2003) 869–899.
[2] K.F.R. Santos, S.M. Shishido, F.R. Laurindo, M.G. de Oliveira, M.H. Krieger, Characterization of the hypotensive effect of *S*-nitroso-*N*-acetylcysteine in normotensive and hypertensive conscious rats, Nitric Oxide 7 (2002) 57–66.
[3] V. Sorrenti, C. Di Giacomo, L. Salermo, M.A. Siracusa, F. Guerra, A. Vanella, Inhibition of neuronal nitric oxide synthase by *N*-phenacyl imidazoles, Nitric Oxide 5 (2001) 32–38.
[4] A.R. Rubio, M.A. Morales-Segura, Nitric oxide, ans iceberg in cardiovascular physiology: far beyond vessel tone control, Arch. Med. Res. 35 (2004) 806–812.
[5] J.E. Stern, Y. Li, W. Zhang, Nitric oxide: a local signaling molecule controlling the activity of pre-autonomic neurons in the paraventricular nucleus of the hypothalamus, Acta Physiol. Scand. 117 (2003) 37–42.
[6] N. Hopkins, E. Cadogan, S. Giles, J. Bannigan, P. McLoughlin, Type 2 nitric oxide synthase and protein nitration in chronic lung infection, J. Phatol. 199 (2003) 122–129.
[7] W. Wang, S. Jittikanont, S.A. Falk, P. Li, L.L. Feng, P.E. Gengaro, B.D. Poole, R.P. Bowler, B.J. Day, J.D. Crapo, R.W. Schrier, Interaction among nitric oxide, reactive oxygen species and antioxidants during endotoxemia-related acute renal failure, Am. J. Physiol-Renal 284 (2003) 532–537.
[8] E. Sanz, N. Fernandez, L. Monge, M.A. Martinez, B. Climent, G. Dieguez, A.L. Garcia-Villalon, Effects of diabetes on the vascular response to nitric oxide and constrictor prostanoids; gender and regional differences, Life Sci. 72 (2003) 1537–1547.
[9] M.M. Bezerra, S.D. Brain, S. Greenacre, S.M.B. Jeronimo, L.B. de Melo, J. Keeble, F.A.C. da Rocha, Reactive nitrogen species scavenging, rather than nitric oxide inhibition, protects from articular cartilage damage in rat zymosan-induced arthritis, Br. J. Pharmacol. 141 (2004) 172–182.

[10] M.R. Raspollini, G. Amuni, A. Villanucci, V. Boddi, A. Taddei, G.L. Taddei, Expression of inducible nitric oxide synthase and cyclooxygenase-2 in ovarian cancer: correlation with clinical outcome, Gynecol. Oncol. 92 (2004) 806–812.
[11] L.J. Ignarro, C. Napoli, J. Loscalzo, Nitric oxide and cardiovascular agents modulating the bioactivity of nitric oxide an overview, Circ. Res. 90 (2002) 21–28.
[12] A.B. Seabra, A. Fitzpatrick, J. Paul, M.G. de Oliveira MG, R. Weller, Topically applied *S*-nitrosothiol-containing hydrogels as experimental and pharmacological NO donors in human skin, Br. J. Dermatol. (2004) (in press).
[13] F.G. Marcondes, A.A. Ferro, A. Souza-Torsoni, M. Sumitani, M.J. Clark, D.W. Franco, E. Tfouni, M.H. Krieger, In vivo effects of the controlled NO donor/scavenger ruthenium cyclam complexes on blood pressure, Life Sci. 70 (2002) 2735–2752.
[14] M.G. de Oliveira, S.M. Shishido, A.B. Seabra, N.H. Morgon, Thermal stability of primary *S*-nitrosothiols; roles of autocatalysis and structural effects on the rate of nitric oxide release, J. Phys. Chem. A 106 (2002) 8963–8970.
[15] J.S. Stamler, D.J. Singel, J. Loscalzo, Biochemistry of nitric oxide and its redox-activated forms, Science 258 (1992) 1898–1902.
[16] D. Giustarini, A. Milzani, R. Colombo, I. Dalle-Donne, R. Rossi, Nitric oxide and *S*-nitrosothiols in human blood, Clin. Chim. Acta 330 (2003) 85–98.
[17] G. Polat, G. Slan, G.H. Eskandari, N. Delialioglu, O. Bagdatoglu, U. Atik, The role of nitric oxide and lipid peroxidation in patients with plasmodium vivax malaria, Parasite 9 (2002) 371–374.
[18] A.P. Adhuna, A.P. Saltora, R. Bhatnagar, Nitric oxide induced expression of stress proteins in virulent and avirulent promastigotes of *Leishmania donovani*, Immunol. Lett. 71 (2000) 171–176.
[19] P.D. Wood, B. Mutus, R.W. Redmond, The mechanism of photochemical release of nitric oxide from *S*-nitrosoglutathione, Photochem. Photobiol. 64 (1996) 518–524.
[20] S.M. Shishido, M.G. de Oliveira, Polyethylene glycol matrix reduces the rates of photochemical and thermal release of nitric oxide from *S*-nitroso-*N*-acethylcysteine, Photochem. Photobiol. 71 (2000) 273–280.
[21] A.B. Seabra, M.G. de Oliveira, Poly(vinyl alcohol) and poly(vinyl pyrrolidone) blended films for local nitric oxide release, Biomaterials 25 (2004) 3773–3782.
[22] Y. Kodera, A. Matsushima, M. Hiroto, H. Nishimura, A. Ishii, T. Ueno, Y. Inada, Pegylation of proteins and bioactive substances for medical and technical applications, Prog. Polym. Sci. 23 (1998) 1233–1271.
[23] V.L. Deckert, S. Duverneuil, S. Poupon, S. Monier, N. Leguern, G. Lizard, D. Masson, L. Lagrost, The impairment of endothelium-dependent arterial relaxation by 7-ketocholesterol is associated with an early activation of protein kinase C, Br. J. Pharmacol. 137 (2002) 655–662.
[24] K. Nakai, H. Togashi, T. Yasukohchi, I. Sakuma, S. Fujii, M. Yoshioka, H. Satoh, A. Kitabatake, Preparation and characterization of SNO–PEG–hemoglobin as a candidate for oxygen transporting material, Int. J. Artif. Organs 24 (2001) 322–328.
[25] S. Walsh, A. Shah, J. Mond, Improved pharmacokinetics and reduced antibody reactivity of lysostaphin conjugated to polyethylene glycol, Antimicrob. Agents Chemother. 74 (2003) 554–558.
[26] S.H. Baysal, A.H. Uslan, Encapsulation of catalase and PEG-catalase in erythrocyte, Artif. Cells Blood Substit. Immobil. Biotechnol. 29 (2001) 359–366.
[27] R.B. Greenwald, PEG drugs: an overview, J. Control. Release 74 (2001) 159–171.
[28] X.Y. Chen, R. Park, A.H. Shahinian, J.R. Bading, P.S. Conti, Pharmacokinetics and tumor retention of I-125-labeled RGD peptide are improved by pegylation, Nucleic Med. Biol. 31 (2004) 11–19.
[29] K.S. Bolh, J.L. West, Nitric oxide-generating polymers reduce platelet adhesion and smooth muscle cell proliferation, Biomaterials 21 (2000) 2273–2278.
[30] S.M. Shishido, A.B. Seabra, W. Loh, M.G. de Oliveira, Thermal and photochemical nitric oxide release from *S*-nitrosothiols incorporated in pluronic F-127 gel: potential uses for local and controlled nitric oxide release, Biomaterials 24 (2003) 3543–3553.
[31] Y.M. Xu, Y.M. Du, Effect of molecular structure of chitosan on protein delivery properties of chitosan nanoparticles, Int. J. Pharm. 250 (2003) 215–226.
[32] A. Vila, A. Sanchez, C. Perez, M.J. Alonso, PLA–PEG nanospheres: new carrier for transmucosal delivery of protein and plasmid DNA, Polym. Adv. Technol. 13 (2002) 851–858.
[33] J.X. Zhang, C.B. Hansen, T.M. Allen, A. Boey, R. Boch, Lipid-derivatized poly(ethylene glycol) micellar formulations of benzoporphyrin derivatives, J. Control. Release 86 (2003) 323–338.
[34] A.N. Lukyanov, V.P. Torchilin, Micelles from lipid derivatives of water-soluble polymers as delivery systems for poorly soluble drugs, Adv. Drug Deliver Rev. 56 (2004) 1273–1289.
[35] S. Sharma, R.W. Johnson, T.A. Desai, Ultrathin poly(ethylene glycol) films for silicon-based microdevices, Appl. Surf. Sci. 206 (2003) 218–229.
[36] D.L.H. Williams, The chemistry of *S*-nitrosothiols, Acc. Chem. Res. 32 (1999) 869–876.
[37] D.J. Sexton, A. Muruganandam, D.J. McKenney, B. Mutus, Visible light photochemical release of nitric oxide from *S*-nitrosoglutathione: potential photochemotherapeutic applications, Photochem. Photobiol. 59 (1994) 463–467.
[38] K. Matsunaga, R.F. Furchgott, Interactions of light and sodium nitrite in producing relaxation of rabbit aorta, J. Pharmacol. Exp. Ther. 248 (1989) 687–695.
[39] M.A. Mendes, R.S. Pimpim, T. Kotiaho, M.N. Eberlin, A cryotrap membrane introduction mass spectrometry system for analysis of volatile organic compounds in water at the low parts-per-trillion level, Anal. Chem. 68 (1996) 3502–3506.
[40] R.M. Alberici, M.A. Mendes, W.F. Jardim, M.N. Eberlin, Mass spectrometry on-line monitoring and MS2 product characterization of TiO_2/UV photocatalytic degradation of chlorinated volatile organic compounds, J. Am. Soc. Mass Spectrom. 9 (1998) 1321–1327.
[41] R.M. Alberici, M.C. Canela, M.N. Eberlin, W.F. Jardim, Catalyst deactivation in the gas phase destruction of nitrogen-containing organic compounds using TiO_2/UV–Vis, Appl. Catal. B. Environ. 30 (2001) 389–397.
[42] M.C. Canela, R.M. Alberici, R.C.R. Sofia, M.N. Eberlin, W.F. Jardim, Destruction of malodorous compounds using heterogeneous photocatalysis, Environ. Sci. Technol. 33 (1999) 2788–2792.
[43] M.G. de Oliveira, J. Langley, A.J. Rest, Photolysis of the $[Fe(CN)_5(NO)]^{2-}$ ion in water and poly(vinyl alcohol) films: evidence for cyano radical, cyanide ion and nitric oxide loss and redox pathways, J. Chem. Soc. Dalton Trans. (1995) 2013–2019.
[44] J. Sun, X.J. Zhang, M. Broderick, H. Fein, Measurement of nitric oxide production in biological systems by using Griess reaction assay, Sensor 3 (2003) 276–284.
[45] J.K.J. Park, P. Kostka, Fluorimetric detection of biological *S*-nitrosothiols, Anal. Biochem. 249 (1997) 61–66.
[46] K. Shibuki, An electrochemical microprobe for detecting nitric oxide release in brain tissue, Neurosci. Res. 9 (1990) 69–76.
[47] R.M. Bateman, C.G. Ellis, D.J. Freeman, Optimization of nitric oxide chemiluminescence operating conditions for measurement of plasma nitrite and nitrate, Clin. Chem. 48 (2002) 570–573.
[48] H.C. Ansel, L.V. Allen, N.G. Popovich, Transdermal drug delivery systems, in: D. Balado (Ed), Pharmaceutical Dosage forms and Drug Delivery Systems, Maryland, pp. 263–278.